BAU Journal - Science and Technology

Volume 4 | Issue 2
ISSN: 2959-331X

Article 6

June 2023

ADSORPTION PERFORMANCE OF MG0.33NI0.33CO0.33FE2O4 NANOPARTICLES DOPED WITH GADOLINIUM AND LANTHANUM FOR LEAD (II) REMOVAL

Mariam Rabaa
Departement of Chemistry, Faculty of Science, Beirut Arab University, Debbieh, Lebanon, mariam_rabaa@hotmail.com

Amani Aridi
Departement of Chemistry, Faculty of Science, Beirut Arab University, Debbieh, Lebanon, a.aridi@bau.edu.lb

Ghassan Younes
Departement of Chemistry, Faculty of Science, Beirut Arab University, Debbieh, Lebanon, ghass@bau.edu.lb

Ramadan Awad
Departement of Physics, Faculty of Science, Beirut Arab University, Debbieh, Lebanon, ramadan.awad@bau.edu.lb

Recommended Citation

Rabaa, Mariam; Aridi, Amani; Younes, Ghassan; and Awad, Ramadan (2023) "ADSORPTION PERFORMANCE OF MG0.33NI0.33CO0.33FE2O4 NANOPARTICLES DOPED WITH GADOLINIUM AND LANTHANUM FOR LEAD (II) REMOVAL," *BAU Journal - Science and Technology*: Vol. 4: Iss. 2, Article 6.
DOI: https://doi.org/10.54729/2959-331X.1098

1. INTRODUCTION

Heavy metal pollution is a serious environmental problem on a global scale (Mosleh et al., 2022). Being non-biodegradable, heavy metals can accumulate in plants and animals and reach humans through a different ways, including the skin, respiration, and the food chain (Zou et al., 2019). Health concerns result from heavy metal ions entering water and food systems even in low concentrations. Lead ions (Pb(II)) are one of the most common heavy metals produced in, glass production, copper mining, battery production and metal plating (Khanniri et al., 2021). After entering to human body, Pb (II) accumulates in the bones, kidney, muscles and brain which may cause, anemia, anorexia and damage to the nervous system (Briffa et al., 2020; Kumar et al., 2020). Due to its high toxicity even at low concentration, the world health organization established a maximum allowed concentration of the Pb (II) ions in drinking water as 10 $\mu g.L^{-1}$ (Chowdhury et al., 2022). Since heavy metals endanger the human health, their elimination from water is extremely required. Consequently, several technologies have been used to remove heavy metals ions, including chemical precipitation, adsorption, ion exchange and membrane filtration (Ince & Ince, 2019; Peng & Guo, 2020; Tahir et al., 2019). Adsorption is one of the most often applied method, among the previously listed methods, because of its low cost and ease of usage (Chai et al., 2021; Rajabi et al., 2023).

Recently, spinel ferrite nanoparticles have been applied in numerous environmental applications such as the degradation of dyes and organic pollutants and the elimination of heavy metals (Jayalakshmi et al., 2022). This is owed to their small particle size, dispersity, large surface area and magnetic properties (Zahid et al., 2019). Saeid et al. (Saeid & Ateia, 2022) reported improved adsorption activity of samarium and gadolinium doped calcium nano ferrite where 99.31 % of Pb (II) was removed from wastewater. In addition, 35% and 80 % of Pb (II) was removed in the presence of $Mg_{1-x}Ni_xFe_2O_4$ and $CoFe_2O_4$ nanoparticles (Putri et al., 2019; Sreekala et al., 2021). Doping spinel ferrite nanoparticles with rare earth metals improve their properties (Jadhav et al., 2023; Taneja et al., 2022). Based on the above background, this study evaluates the adsorption performance of $Mg_{0.33}Ni_{0.33}Co_{0.33}Gd_xFe_{2-x}O_4$ and $Mg_{0.33}Ni_{0.33}Co_{0.33}La_xFe_{2-x}O_4$ nanoparticles where x = 0.00, 0.01 and 0.08 for the removal of Pb (II).

2. METHODS AND MATERIALS

2.1 Preparation of Gd and La-doped $Mg_{0.33}Ni_{0.33}Co_{0.33}Gd_xFe_{2-x}O_4$ Nanoparticles

$Mg_{0.33}Ni_{0.33}Co_{0.33}Gd_xFe_{2-x}O_4$ and $Mg_{0.33}Ni_{0.33}Co_{0.33}La_xFe_{2-x}O_4$ nanoparticles where x = 0.00, 0.01 and 0.08 were prepared by the co-precipitation method. Appropriate amounts of $CoCl_2.H_2O$, $NiCl_2.6H_2O$, $MgCl_2.6H_2O$, $GdCl_3.6H_2O$, $LaCl_3.6H_2O$ and $FeCl_3.6H_2O$ were dissolved in distilled water at room temperature. The chloride solutions were mixed at room temperature. Then, NaOH solution (3 M) was added dropwise until adjusting the pH to 12. While stirring the mixture magnetically, the resulting solution was heated at 80 ℃. After that, the precipitates were filtered and washed until pH 7. The precipitates were dried at 100 ℃ for approximately 18 hours. Lastly, dried powders were annealed for 4 hours at 550 ℃.

2.2 Characterization Techniques

X-ray diffraction (XRD) and transmission electron microscopy (TEM) analysis were performed to evaluate the structural properties of the prepared nanoparticles. Thus, D8 Focus Bruker was used to perform the XRD analysis using Cu-kα radiation source (λ = 1.54056 Å) in the range of $20° \leq 2\theta \leq 80°$. TEM analysis was performed via JEM-1400 Plus. The optical properties of the prepared nanoparticles were assessed by ultraviolet-visible (UV-Vis) spectroscopic measurements that were recorded between 300 and 700 nm using V-670 spectrophotometer.

2.3 Removal of Pb (II)

The adsorption performance of $Mg_{0.33}Ni_{0.33}Co_{0.33}Gd_xFe_{2-x}O_4$ and $Mg_{0.33}Ni_{0.33}Co_{0.33}La_xFe_{2-x}O_4$ nanoparticles, where x = 0.00, 0.01 and 0.08, was evaluated for the removal of Pb (II). 5 ppm of Pb (II) solution was prepared by serial dilution of stock 1000 ppm solutions. The pH of the 5 ppm Pb (II) solution is 2.6. After weighing 40 mg of each sample, they were mixed with 50 mL of the 5 ppm Pb (II) solutions using a sonicator. Then, 5 mL of the solution were removed from the reaction at different time intervals and analyzed using Atomic Absorption Spectroscopy. The effect of the Pb (II) concentration was studied. The removal % was estimated using the following relation:

$$\text{Removal \%} = \frac{C_0 - C_t}{C_0} \times 100 \qquad (1)$$

3. RESULTS AND DISCUSSION

3.1 Structural and Optical Properties of the Prepared Nanoparticles

The XRD patterns for $Mg_{0.33}Ni_{0.33}Co_{0.33}Gd_xFe_{2-x}O_4$ and $Mg_{0.33}Ni_{0.33}Co_{0.33}La_xFe_{2-x}O_4$ nanoparticles where x= 0.00, 0.01 and 0.08 are shown in Fig. 1. The observed peaks are indexed by a cubic spinel phase with space group Fd3m. In addition, the XRD patterns are well matched with the standard JCPDS card no. 36-0398 (Ajeesha et al., 2021). The presence of an extra peak in the XRD pattern of pure $Mg_{0.33}Ni_{0.33}Co_{0.33}Fe_2O_4$ nanoparticles (x = 0.00) confirms the presence of hematite as a secondary phase. Though, the intensity of this peak starts to decrease as the Gd and La content increase. The absence of extra peaks in the XRD patterns of the prepared doped nanoparticles confirms the purity of the prepared samples. The values of the lattice parameter (a) are listed in Table 1.

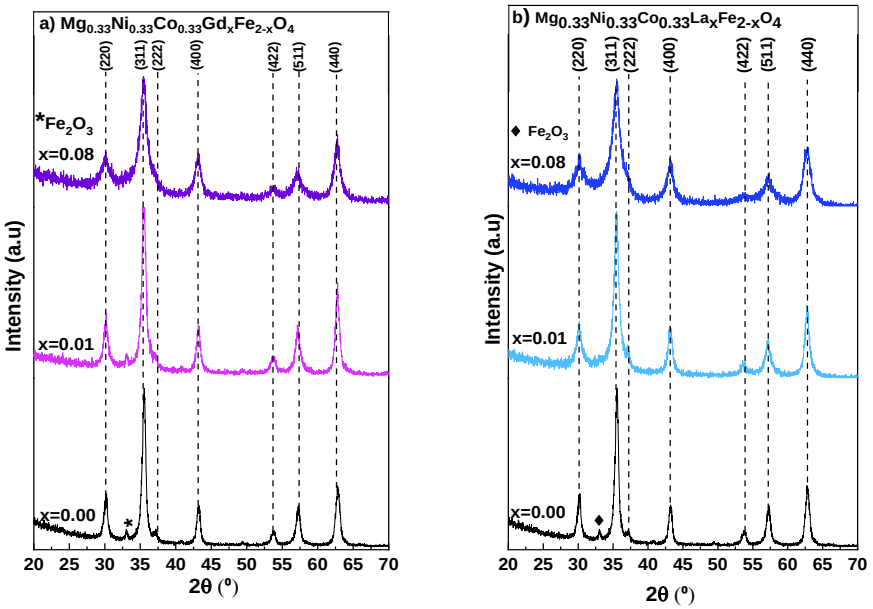

Fig.1: XRD patterns of (a) $Mg_{0.33}Ni_{0.33}Co_{0.33}Gd_xFe_{2-x}O_4$ and (b) $Mg_{0.33}Ni_{0.33}Co_{0.33}La_xFe_{2-x}O_4$ nanoparticles where x = 0.00, 0.01 and 0.08.

TEM images and particle size distribution of $Mg_{0.33}Ni_{0.33}Co_{0.33}Gd_xFe_{2-x}O_4$ and $Mg_{0.33}Ni_{0.33}Co_{0.33}La_xFe_{2-x}O_4$ nanoparticles are demonstrated in Fig. 2. The prepared nanoparticles exhibit spherical morphology. In addition, as Gd and La content increases from 0.00 to 0.08, the average particle sizes decrease from 28.7 to 21.2 and 20.2 nm, respectively.

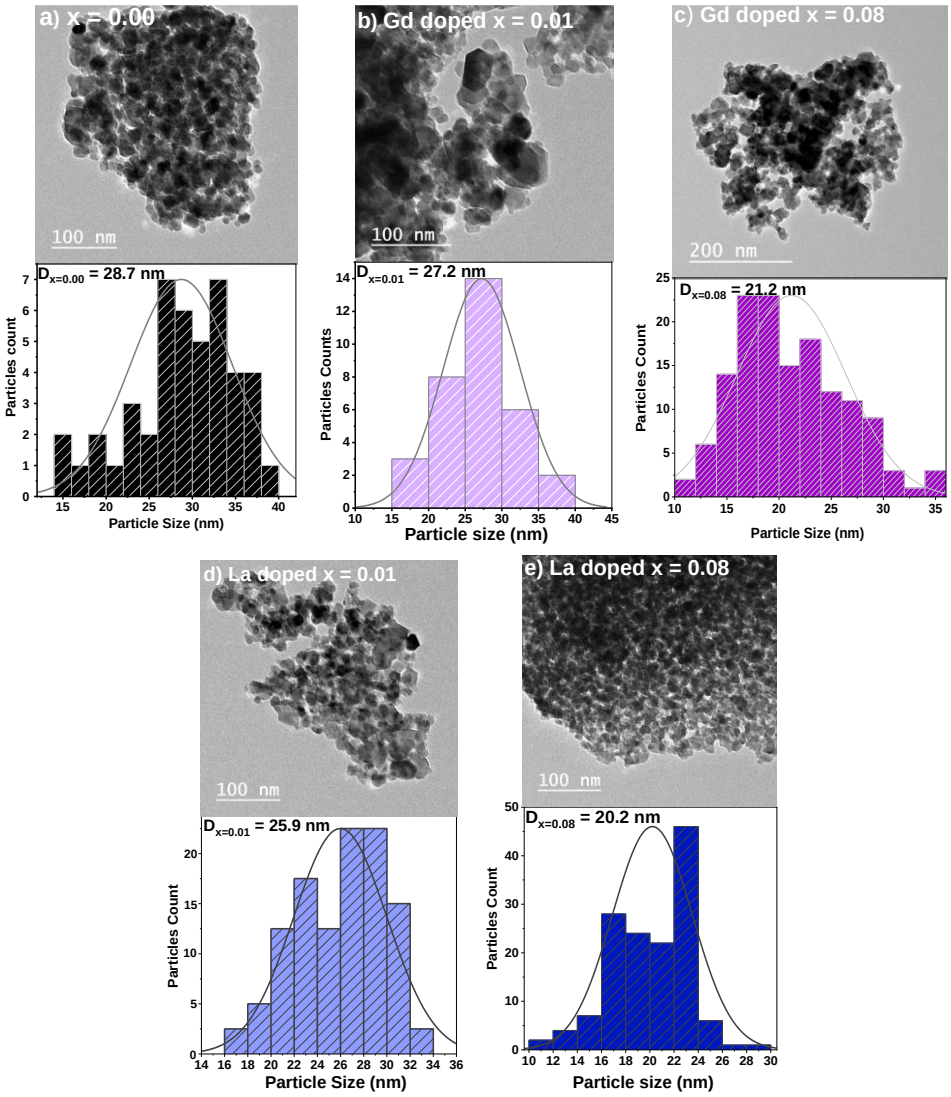

Fig.2:TEM images and particle size distribution of (a) $Mg_{0.33}Ni_{0.33}Co_{0.33}Fe_2O_4$ (x=0.00) nanoparticles, $Mg_{0.33}Ni_{0.33}Co_{0.33}Gd_xFe_{2-x}O_4$ with (b) x = 0.01 and (c) x=0.08 and $Mg_{0.33}Ni_{0.33}Co_{0.33}La_xFe_{2-x}O_4$ with (d) x = 0.01 and (e) x=0.08.

The specific surface area is an important property that makes nanoparticles versatile and useful for a wide range of applications in various fields such as catalysis and adsorption of heavy metals. Thus, the specific surface area (S) of the prepared nanoparticles was calculated by applying the following equation (Basma et al., 2022):

$$S = \frac{6000}{\rho \times D}, \qquad (2)$$

where ρ represents the X-ray density and D denotes the average particle size determined from TEM analysis. The X-ray density (ρ) was calculated from the following relation (Al Boukhari et al., 2020):

$$\rho = \frac{8\,M}{N_A \times a^3}, \qquad (3)$$

knowing that M, N_A and a represents is the molar mass, Avogadro's number and lattice parameter of the prepared nanoparticles, respectively. The obtained values of a, M, ρ and S are listed in Table 1. The specific surface area (S) increases from 41.12 to 54.12 and 57.26 m^2/g as Gd and La content increases from 0.00 to 0.08, respectively.

Table 1: The values of lattice parameter (a), Molar mass (M), X-ray density (ρ) and specific surface area (S) of $Mg_{0.33}Ni_{0.33}Co_{0.33}Gd_xFe_{2-x}O_4$ and $Mg_{0.33}Ni_{0.33}Co_{0.33}La_xFe_{2-x}O_4$ nanoparticles, where x= 0.00, 0.01 and 0.08

x	a (Å)	M (g/mol)	ρ (g/cm^3)	S (m^2/g)
0.00	8.351(3)	222.52	5.0752	41.19
$Mg_{0.33}Ni_{0.33}Co_{0.33}Gd_xFe_{2-x}O_4$				
0.01	8.361(9)	223.54	5.0789	43.43
0.08	8.367(8)	230.64	5.2292	54.12
$Mg_{0.33}Ni_{0.33}Co_{0.33}La_xFe_{2-x}O_4$				
0.01	8.366(5)	223.35	5.0664	45.72
0.08	8.372(5)	229.17	5.1871	57.26

The optical properties of $Mg_{0.33}Ni_{0.33}Co_{0.33}Gd_xFe_{2-x}O_4$ and $Mg_{0.33}Ni_{0.33}Co_{0.33}La_xFe_{2-x}O_4$ nanoparticles, where x= 0.00, 0.01 and 0.08, are evaluated via UV-vis spectroscopy. The absorption spectra were recorded in the range of 300 - 700 nm and shown in Fig. 3 (a and b). In pure and doped nanoparticles, a major peak appeared around 336 nm. Comparable UV spectra of ferrite nanoparticles, mainly $Ni_{1-x}Mg_xFe_2O_4$ nanoparticles are reported in a previous study (Chavan & Naik, 2017). It is noticeable that as Gd and La content increases, the intensity of the peak increases.

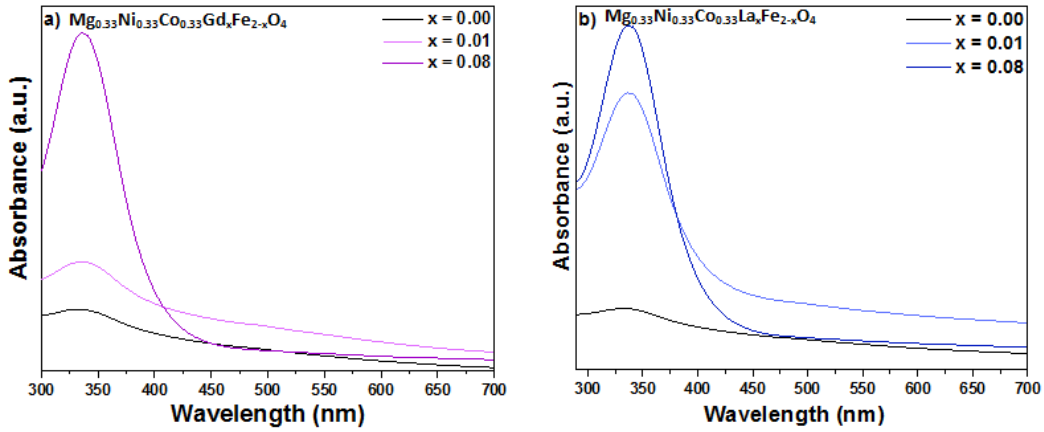

Fig. 3 UV-vis spectra of (a) $Mg_{0.33}Ni_{0.33}Co_{0.33}Gd_xFe_{2-x}O_4$ and (b) $Mg_{0.33}Ni_{0.33}Co_{0.33}La_xFe_{2-x}O_4$ nanoparticles with x = 0.00, 0.01 and 0.08.

The bandgap energy (E_g) was valued from Tauc's plot by using in the following relation:

$$(\alpha h\upsilon)^2 = A\,(h\upsilon - E_g)\,, \qquad (4)$$

where α, $h\upsilon$ and A represent the absorption coefficient, photon energy and transition probability constant, respectively. Thus, the bandgap energy (E_g) was determined by plotting $(\alpha h\upsilon)^2$ versus $h\upsilon$ and the obtained results are shown in Figs. 4 (a and b) and Table 2. Upon doping nanoparticles with Gd and La E_g values increased from 2.915 to 3.231 eV and from 2.915 to 3.246 eV, respectively. Thus, the decrease in the particle size revealed from TEM analysis and increase in the bandgap energy upon doping nanoparticles with Gd and La is owed to the quantum size effect.

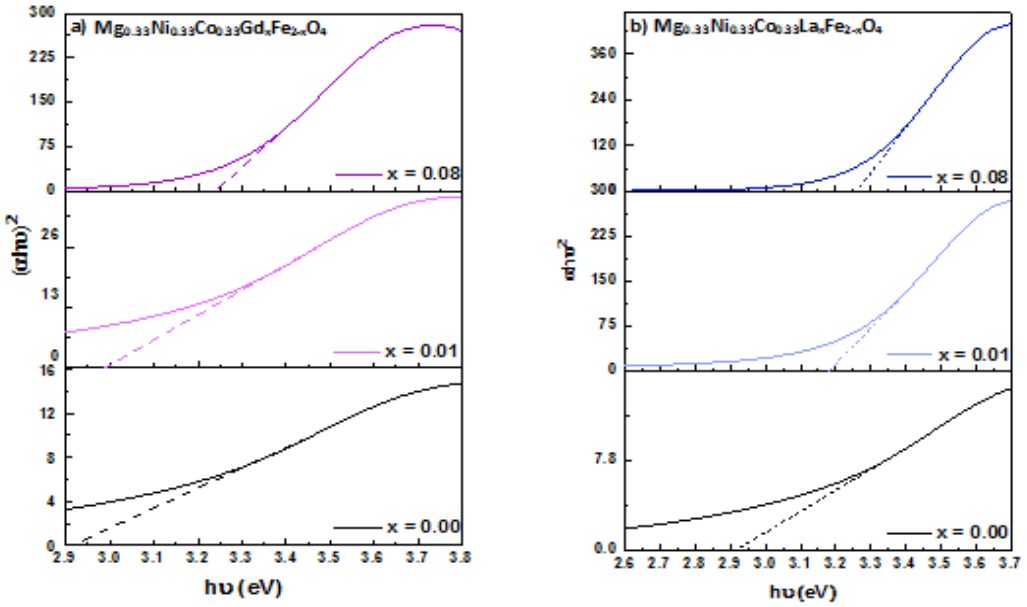

Fig.4: Tauc's plot of (a) $Mg_{0.33}Ni_{0.33}Co_{0.33}Gd_xFe_{2-x}O_4$ and (b) $Mg_{0.33}Ni_{0.33}Co_{0.33}La_xFe_{2-x}O_4$ nanoparticles where x=0.00, 0.01 and 0.08.

Table 2 E_g and E_U values of $Mg_{0.33}Ni_{0.33}Co_{0.33}Gd_xFe_{2-x}O_4$ and $Mg_{0.33}Ni_{0.33}Co_{0.33}La_xFe_{2-x}O_4$ nanoparticles where x = 0.00, 0.01 and 0.08

x	E_g (eV)	E_U (eV)
0.00	2.915	1.322
$Mg_{0.33}Ni_{0.33}Co_{0.33}Gd_xFe_{2-x}O_4$		
0.01	2.981	1.138
0.08	3.231	0.327
$Mg_{0.33}Ni_{0.33}Co_{0.33}La_xFe_{2-x}O_4$		
0.01	3.217	0.487
0.08	3.246	0.306

The Urbach energy (E_U) is correlated with the defect or disorder in the prepared nanoparticles and it is determined from the following equation:

$$\ln(\alpha) = \ln(\alpha_0) + \frac{h\upsilon}{E_U}, \qquad (5)$$

where α_0 is a constant. Consequently, E_U is the reciprocal slope of the plot of ln (α) versus (hυ). The obtained plots and E_U values are represented in Figs. 5 (a and b) and listed in Table 2. The doped samples exhibited lower E_U values compared to that of pure nanoparticles, where x=0.00. Furthermore, an inverse proportionality between E_U and E_g was observed. Similar behavior was reported in a previous study for La-doped $ZnFe_2O_4$ (Lemziouka et al., 2020).

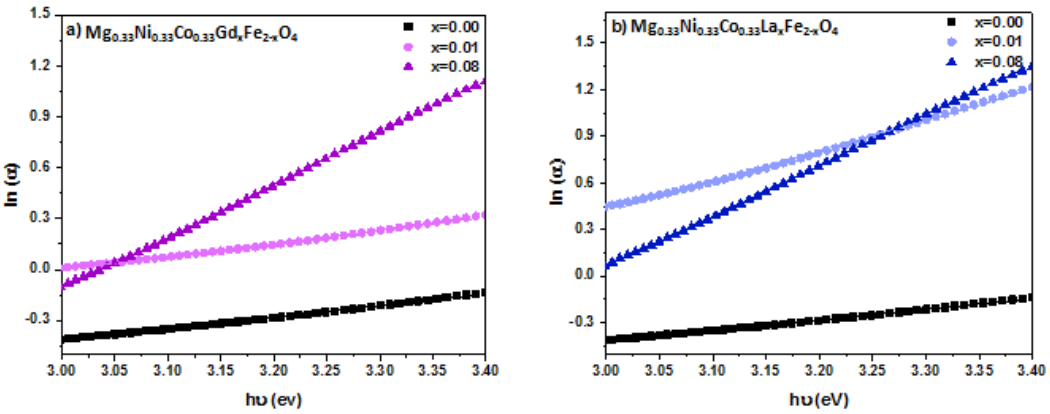

Fig.5: Plots for E_U determination of (a) $Mg_{0.33}Ni_{0.33}Co_{0.33}Gd_xFe_{2-x}O_4$ and (b) $Mg_{0.33}Ni_{0.33}Co_{0.33}La_xFe_{2-x}O_4$ nanoparticles where x=0.00, 0.01 and 0.08.

The following equation was applied to determine the variation of the extinction coefficient (k) with wavelength (λ) (Lemziouka et al., 2020):

$$k = \frac{\alpha \lambda}{4\pi}. \qquad (6)$$

The results are displayed in Fig. 6 (a and b). For all the prepared nanoparticles, the extinction coefficient (k) increases to its maximum value as wavelength increases to reach 335 nm and then decreases. Furthermore, the extinction coefficient values of Gd and La-doped samples are greater than that of pure nanoparticles. This might be attributed to the increase in the absorption coefficient revealing the occurrence of direct electronic transitions (Faramawy et al., 2022; Lemziouka et al., 2020).

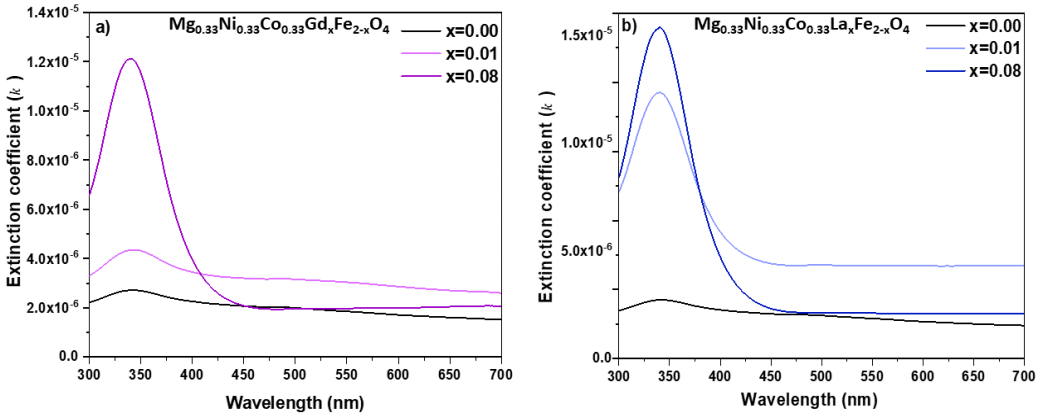

Fig.6: Variation of the extinction coefficient (k) against wavelength for (a) $Mg_{0.33}Ni_{0.33}Co_{0.33}Gd_xFe_{2-x}O_4$ and (b) $Mg_{0.33}Ni_{0.33}Co_{0.33}La_xFe_{2-x}O_4$ nanoparticles where x = 0.00, 0.01 and 0.08.

The refractive index (n) is an important factor in evaluating the optical and electric properties of a semiconductor (Massoudi et al., 2020). It can be determined from the following equation:

$$n = \frac{1}{T_s} + \left(\frac{1}{T_s - 1}\right)^{1/2}, \qquad (7)$$

where TS is the percentage transmission coefficient. The variation of the refractive index (n) against wavelength for Mg0.33Ni0.33Co0.33GdxFe2-xO4 and Mg0.33Ni0.33Co0.33LaxFe2-xO4 nanoparticles are represented in Figs. 7 (a and b). The refractive index increases as the wavelength increases to reach 335 nm. With further increase in the wavelength to reach 700 nm, the refractive index decreases. Furthermore,

the refractive index is greatly increased upon doping the nanoparticles with Gd and La. Hence, doping Mg0.33Ni0.33Co0.33Fe2-xO4 nanoparticles with Gd and La play an important role in enhancing the k and n values, which in turn improve the optical properties of nanoparticles and enable their usage in optoelectronic applications (Lemziouka et al., 2020).

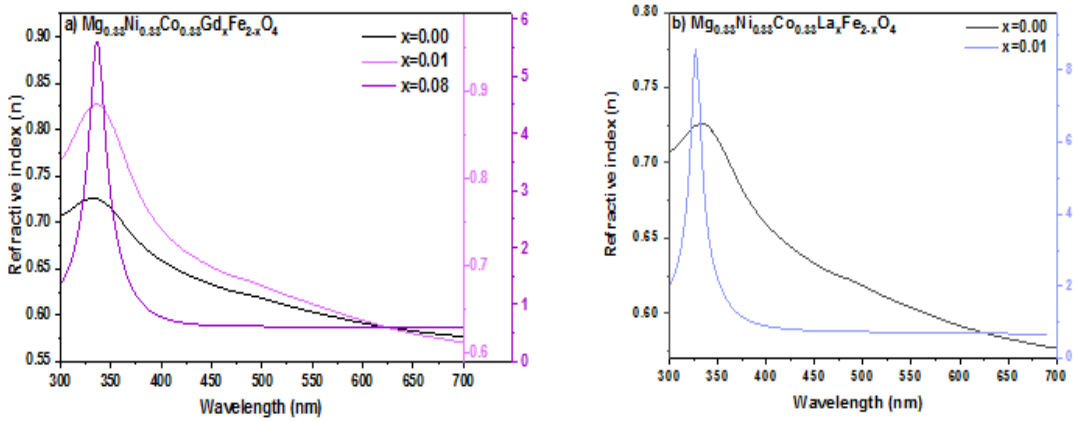

Fig.7: Variation of the refractive index (n) against wavelength for (a) $Mg_{0.33}Ni_{0.33}Co_{0.33}Gd_xFe_{2-x}O_4$ and (b) $Mg_{0.33}Ni_{0.33}Co_{0.33}La_xFe_{2-x}O_4$ nanoparticles where x = 0.00, 0.01 and 0.08.

3.1. Removal of Pb (II)

The efficiency of $Mg_{0.33}Ni_{0.33}Co_{0.33}Gd_xFe_{2-x}O_4$ and $Mg_{0.33}Ni_{0.33}Co_{0.33}La_xFe_{2-x}O_4$ nanoparticles where x = 0.00, 0.01 and 0.08 for the removal of heavy metals was evaluated. This was done by analyzing the adsorption of Pb (II) onto the nanoparticles' surface as a function of contact time as shown in Fig. 8 and 9. For all the prepared samples, as contact time increases from 30 to reach 90 min, the removal % of Pb (II) increases. Furthermore, doping $Mg_{0.33}Ni_{0.33}Co_{0.33}Fe_2O_4$ with Gd improved the adsorption performance of nanoparticles. However, the highest removal % was achieved in the presence of $Mg_{0.33}Ni_{0.33}Co_{0.33}Gd_xFe_{2-x}O_4$ NPs with x = 0.01 where around 75 % of Pb (II) were removed after 90 min, as shown in Fig. 3. For La-doped nanoparticles, as La content increases from x = 0.00 to 0.01, the removal % decreases from 38 % to reach 16 % after contact time of 90 min. Whereas with further increase in the La content to reach 0.08, the removal % increases to reach 41 % after 90 min. Compared with previously published papers, superior adsorption activity was achieved in presence of $Mg_{0.33}Ni_{0.33}Co_{0.33}Gd_xFe_{2-x}O_4$ NPs with x = 0.01 as listed in Table 3.

The adsorption of Pb (II) ions on Gd and La doped ferrites can be influenced by the magnetic moment of these materials. Gd-doped ferrites are known to exhibit a high magnetic moment due to the presence of the Gd ions, which have a large magnetic moment (7.9 μB) (Yao et al., 2021). This high magnetic moment can enhance the adsorption of Pb (II) ions on the surface of the ferrite nanoparticles through magnetic interactions. On the other hand, La ions have very low magnetic moment which is less than 1 μB (Kołczyk et al., 2016). This may result in weaker magnetic interactions between the Pb (II) ions and the ferrite surface, leading to a lower adsorption capacity.

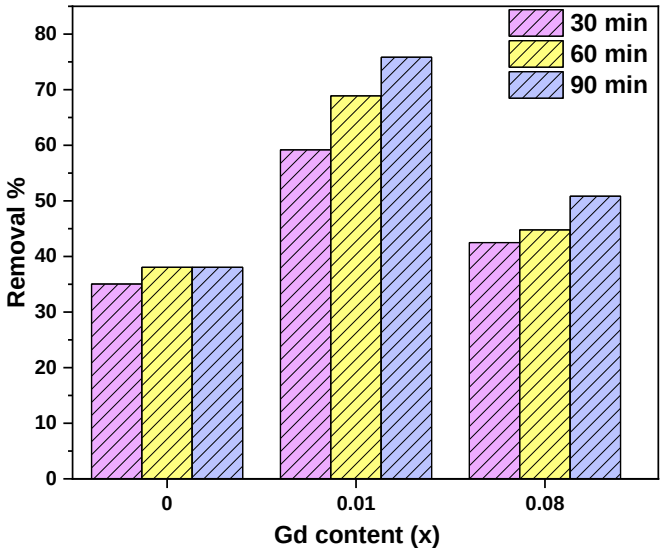

Fig.8: Adsorption of Pb (II) onto the $Mg_{0.33}Ni_{0.33}Co_{0.33}Gd_xFe_{2-x}O_4$ nanoparticles' surface with x = 0.00, 0.01 and 0.08 as a function of contact time.

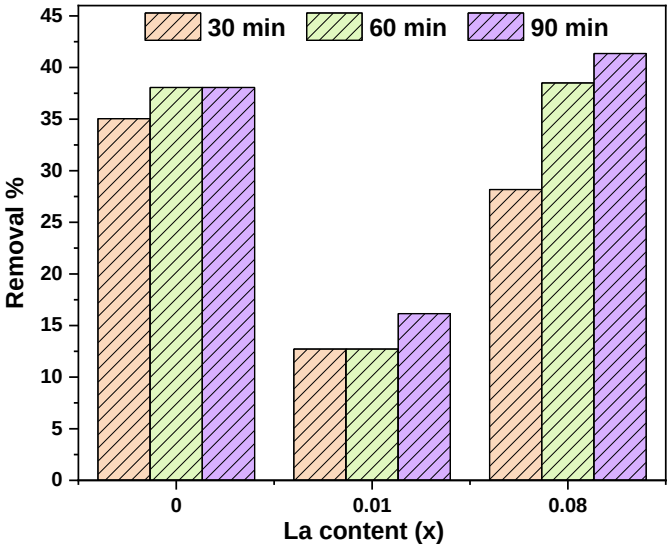

Fig.9: Adsorption of Pb (II) onto the $Mg_{0.33}Ni_{0.33}Co_{0.33}La_xFe_{2-x}O_4$ nanoparticles' surface with x = 0.00, 0.01 and 0.08 as a function of contact time.

Table 3 The removal % of Pb (II) reported in previously published reports and studied in acidic medium in the prescence of several adsorbents

Adsorbent	pH	Removal %	Time (min)	Ref.
$NiFe_2O_4$	3	72 %	120	(Khoso et al., 2021)
γ-Fe_2O_3	4.5	71.29 %	120	(Ahmadi et al., 2014)
$CaFe_2O_4$	3	<10%	60	(Saeid & Ateia, 2022)
$Ni_{0.1}Fe_{2.9}O_4$	3	61 %	60	(Ramadan, 2019)
$Mg_{0.33}Ni_{0.33}Co_{0.33}Gd_{0.01}Fe_{1.99}O_4$	2.6	75 %	90	This Study

4. CONCLUSION

$Mg_{0.33}Ni_{0.33}Co_{0.33}Gd_xFe_{2-x}O_4$ and $Mg_{0.33}Ni_{0.33}Co_{0.33}La_xFe_{2-x}O_4$ nanoparticles with x=0.00, 0.01 and 0.08 were prepared by the co-precipitation method and used as adsorbents for the removal of Pb (II). XRD analysis revealed the purity and spinel structure of the prepared samples. The spherical morphology of the prepared nanoparticles was revealed from TEM images. Furthermore, as Gd and La content increased the particle size and Urbach energy decreased while the bandgap energy increased. Doping nanoparticles with Gd and La enhanced the adsorption performance for the removal of Pb (II). Among the prepared samples, improved adsorption activity was revealed by $Mg_{0.33}Ni_{0.33}Co_{0.33}Gd_xFe_{2-x}O_4$ nanoparticles with x = 0.01 and $Mg_{0.33}Ni_{0.33}Co_{0.33}La_xFe_{2-x}O_4$ nanoparticles with x = 0.08. The results reaffirm the capacity of using ferrites in wastewater treatment particularly in removal of heavy metals.

REFERENCES

- Ahmadi, A., Heidarzadeh, S., Mokhtari, A. R., Darezereshki, E., & Harouni, H. A. (2014). Optimization of heavy metal removal from aqueous solutions by maghemite (γ-Fe2O3) nanoparticles using response surface methodology. *Journal of Geochemical Exploration*, *147*, 151-158.
- Ajeesha, T., Ashwini, A., George, M., Manikandan, A., Mary, J. A., Slimani, Y., . . . Baykal, A. (2021). Nickel substituted MgFe2O4 nanoparticles via co-precipitation method for photocatalytic applications. *Physica B: Condensed Matter*, *606*, 412660.
- Al Boukhari, J., Khalaf, A., Sayed Hassan, R., & Awad, R. (2020). Structural, optical and magnetic properties of pure and rare earth-doped NiO nanoparticles. *Applied Physics A*, *126*, 1-13.
- Basma, H., Al Boukhari, J., Abd Al Nabi, M., Aridi, A., Sayed Hassan, R., Naoufal, D., . . . Awad, R. (2022). Enhancement of the magnetic and optical properties of Ni0. 5Zn0. 5Fe2O4 nanoparticles by ruthenium doping. *Applied Physics A*, *128*(5), 409.
- Briffa, J., Sinagra, E., & Blundell, R. (2020). Heavy metal pollution in the environment and their toxicological effects on humans. *Heliyon*, *6*(9), e04691.
- Chai, W. S., Cheun, J. Y., Kumar, P. S., Mubashir, M., Majeed, Z., Banat, F., . . . Show, P. L. (2021). A review on conventional and novel materials towards heavy metal adsorption in wastewater treatment application. *Journal of Cleaner Production*, *296*, 126589.
- Chavan, P., & Naik, L. (2017). Investigation of energy band gap and conduction mechanism of magnesium substituted nickel ferrite nanoparticles. *physica status solidi (a)*, *214*(9), 1700077.
- Chowdhury, I. R., Chowdhury, S., Mazumder, M. A. J., & Al-Ahmed, A. (2022). Removal of lead ions (Pb2+) from water and wastewater: a review on the low-cost adsorbents. *Applied Water Science*, *12*(8), 185.
- Faramawy, A., Elsayed, H., Scian, C., & Mattei, G. (2022). Structural, Optical, Magnetic and Electrical Properties of Sputtered ZnO and ZnO: Fe Thin Films: The Role of Deposition Power. *Ceramics*, *5*(4), 1128-1153.
- Ince, M., & Ince, O. K. (2019). Heavy metal removal techniques using response surface methodology: water/wastewater treatment. In *Biochemical Toxicology-Heavy Metals and Nanomaterials*. IntechOpen.
- Jadhav, S. A., Somvanshi, S. B., Gawali, S. S., Zakade, K., & Jadhav, K. (2023). Rare earth-doped mixed Ni–Cu–Zn ferrites as an effective photocatalytic agent for active degradation of Rhodamine B dye. *Journal of Rare Earths*.
- Jayalakshmi, R., Jeyanthi, J., & Sidhaarth, K. A. (2022). Versatile application of cobalt ferrite nanoparticles for the removal of heavy metals and dyes from aqueous solution. *Environmental Nanotechnology, Monitoring & Management*, *17*, 100659.

- Khanniri, E., Yousefi, M., Mortazavian, A. M., Khorshidian, N., Sohrabvandi, S., Arab, M., & Koushki, M. R. (2021). Effective removal of lead (II) using chitosan and microbial adsorbents: Response surface methodology (RSM). *International journal of biological macromolecules*, *178*, 53-62.
- Khoso, W. A., Haleem, N., Baig, M. A., & Jamal, Y. (2021). Synthesis, characterization and heavy metal removal efficiency of nickel ferrite nanoparticles (NFN's). *Scientific reports*, *11*(1), 3790.
- Kołczyk, K., Wojnicki, M., Kutyła, D., Kowalik, R., Żabiński, P., & Cristofolini, A. (2016). Separation of Ho3+ in static magnetic field. *Archives of Metallurgy and Materials*, *61*(4), 1919-1924.
- Kumar, A., Kumar, A., MMS, C.-P., Chaturvedi, A. K., Shabnam, A. A., Subrahmanyam, G., . . . Kumar, S. S. (2020). Lead toxicity: health hazards, influence on food chain, and sustainable remediation approaches. *International journal of environmental research and public health*, *17*(7), 2179.
- Lemziouka, H., Boutahar, A., Moubah, R., Omari, L., Bahhar, S., Abid, M., & Lassri, H. (2020). Synthesis, structural, optical and dispersion parameters of La-doped spinel zinc ferrites ZnFe2-xLaxO4 (x= 0.00, 0.001, 0.005, 0.01 and 0.015). *Vacuum*, *182*, 109780.
- Massoudi, J., Smari, M., Nouri, K., Dhahri, E., Khirouni, K., Bertaina, S., & Bessais, L. (2020). Magnetic and spectroscopic properties of Ni–Zn–Al ferrite spinel: from the nanoscale to microscale. *RSC advances*, *10*(57), 34556-34580.
- Mosleh, N., Najmi, M., Parandi, E., Nodeh, H. R., Vasseghian, Y., & Rezania, S. (2022). Magnetic sporopollenin supported polyaniline developed for removal of lead ions from wastewater: Kinetic, isotherm and thermodynamic studies. *Chemosphere*, *300*, 134461.
- Peng, H., & Guo, J. (2020). Removal of chromium from wastewater by membrane filtration, chemical precipitation, ion exchange, adsorption electrocoagulation, electrochemical reduction, electrodialysis, electrodeionization, photocatalysis and nanotechnology: a review. *Environmental Chemistry Letters*, *18*, 2055-2068.
- Putri, W., Setiadi, E., Herika, V., Tetuko, A., & Sebayang, P. (2019). Natural iron sand-based Mg1-xNixFe2O4 nanoparticles as potential adsorbents for heavy metal removal synthesized by co-precipitation method. IOP Conference Series: Earth and Environmental Science,
- Rajabi, M., Keihankhadiv, S., Tyagi, I., Karri, R. R., Chaudhary, M., Mubarak, N. M., . . . Singh, P. (2023). Comparison and interpretation of isotherm models for the adsorption of dyes, proteins, antibiotics, pesticides and heavy metal ions on different nanomaterials and non-nano materials—a comprehensive review. *Journal of Nanostructure in Chemistry*, *13*(1), 43-65.
- Ramadan, R. (2019). Preparation, characterization and application of Ni-doped magnetite. *Applied Physics A*, *125*(9), 586.
- Saeid, Y., & Ateia, E. E. (2022). Efficient removal of Pb (II) from water solution using CaFe2− x− yGdxSmyO4 ferrite nanoparticles. *Applied Physics A*, *128*(7), 583.
- Sreekala, G., Beevi, A. F., Resmi, R., & Beena, B. (2021). Removal of lead (II) ions from water using copper ferrite nanoparticles synthesized by green method. *Materials Today: Proceedings*, *45*, 3986-3990.
- Tahir, M. B., Kiran, H., & Iqbal, T. (2019). The detoxification of heavy metals from aqueous environment using nano-photocatalysis approach: a review. *Environmental Science and Pollution Research*, *26*(11), 10515-10528.
- Taneja, S., Thakur, P., Kumar, R., Hemalatha, S., Slimani, Y., Ravelo, B., & Thakur, A. (2022). Nanostructured Rare Earth Nd3+ doped Nickel–Zinc–Bismuth Spinel Ferrites: Structural, Electrical and Dielectric Studies. *Ceramics International*, *48*(19), 27731-27738.
- Yao, H., Ning, X., Zhao, H., Hao, A., & Ismail, M. (2021). Effect of Gd-doping on structural, optical, and magnetic properties of NiFe2O4 as-prepared thin films via facile sol–gel approach. *ACS omega*, *6*(9), 6305-6311.

- Zahid, M., Nadeem, N., Hanif, M. A., Bhatti, I. A., Bhatti, H. N., & Mustafa, G. (2019). Metal ferrites and their graphene-based nanocomposites: synthesis, characterization, and applications in wastewater treatment. *Magnetic Nanostructures: Environmental and Agricultural Applications*, 181-212.
- Zou, C., Jiang, W., Liang, J., Sun, X., & Guan, Y. (2019). Removal of Pb (II) from aqueous solutions by adsorption on magnetic bentonite. *Environmental Science and Pollution Research*, *26*, 1315-1322